Journal of Materials Chemistry A

COMMUNICATION

View Article Online
View Journal | View Issue

Check for updates

Cite this: J. Mater. Chem. A, 2018, 6, 10649

Received 27th February 2018
Accepted 11th May 2018

DOI: 10.1039/c8ta01906a

rsc.li/materials-a

Published on 11 May 2018. Downloaded by Universidade de Coimbra on 12/19/2018 4:16:09 PM.

Calixarene functionalization of TiO_2 nanoarrays: an effective strategy for enhancing the sensor versatility†

Issam Oueslati, *[abc] Akrem Ghrairi,[c] Edivagner S. Ribeiro,[a] Luís A. E. Batista de Carvalho,[d] João M. Gil[a] and José A. Paixao[a]

Sensitive, selective, low-cost, and simply designed sensors for gases and analytes are highly attractive. The rational synergy between calixarenes (CAs) and titania nanorods (TiO_2NRs) and nanotubes (TiO_2NTs) gives rise to completely new types of behaviors that open unprecedented applications. First, the geometric building of NRs and NTs leads to excellent signal amplification and transduction. Second, grafted CAs create self-assembled monolayers (SAMs) that switch order under a thermal stimulus and generate a stimuli-responsive behavior, thus promoting modulated sensing properties. Third, CAs accelerate gas diffusion in the sensor, yielding a fast, sensitive, selective, and reproducible response to H_2 at room temperature (RT). In addition, these systems may act as sensors for other analytes, such as the pesticide profenofos (PFF).

The fabrication of functional materials requires control in organization of their components with nanometer precision, which can be achieved through dynamic harmonization of atomic-/molecular-level manipulation and control, chemical nanofabrication, self-organization, and field-controlled organization.[1] Controlling these dynamic events is the key to create materials with desirable functions and can be regarded as a central dogma in the development of functional materials. Over the past decade, host–guest complexes have become increasingly targeted as new tools to bind organic molecules onto the surfaces of nanostructured materials, leading to a variety of technologically relevant applications.[2–4] Such systems are promising candidates in the development of selective molecular recognition and surface functionalization due to specific and reversible non-covalent interactions, such as hydrogen bonding, van der Waals forces, π–π stacking interactions, hydrophobic interactions, and electrostatic effects,[5–7] and due to self-assembly.[8–10] In particular, CAs, owing to their availability and easy functionalization at either the upper and/or the lower rim, can selectively bind specific guest molecules. Therefore, grafting CAs on the 3D surface is a convenient strategy to realize functional materials for sensing and separation. A few attempts have been made with metal nanoparticles (NPs), quantum dots, and mesoporous silica,[11] but only one was successful in grafting CAs onto metal nanotubes giving rise to a highly selective and sensitive visible-light-driven sensor.[12]

Among common H_2 sensing materials,[13] TiO_2-based sensors are desired for their inert surface properties and for variation of their electrical resistance upon adsorption of gas.[14] Until now most semiconductor H_2 sensors have shown a weak and slow response, long recovery time at RT, and they require heating to relatively high temperatures for a rapid response rate.[13] To overcome this hindrance, nanofibers, nanorods or their arrays and porous structures of metal oxide semiconductors were developed to improve the hydrogen sensing performance at RT.[15–17] Doping noble metals or combining metal oxide semiconductors with inorganic materials such as monolayer MoS_2 is another possible method to enhance the gas sensing ability.[18–20] But the selectivity problem is not easy to solve because the sensing mechanism depends on the surface reactions.[21] Because CAs are sensitive and specific for gas detection due to their porous structure,[22] CA functionalization of TiO_2 arrays would become an effective route to improve the hydrogen sensing performance at RT and the selectivity. Therefore, how to prepare sensors which show both acceptable sensitivity and fast response–recovery time at or near RT has become an important issue now.[13] An even more challenging issue is turning these sensors selective.

The components of the prepared materials are CAs **1–3** grafted on TiO_2NRs (CA@TiO_2NRs). **1**-Grafted TiO_2NTs (**1**@TiO_2NTs) are prepared for comparison and for study of the effect of thermal stimulus on surface organization. The

[a]CFisUC, Department of Physics, University of Coimbra, P-3004-516 Coimbra, Portugal. E-mail: iooueslati@uc.pt

[b]Mediterranean Institute of Technology, South Mediterranean University, 1053 Tunis, Tunisia

[c]LANSER, CRTEn, Hammam-Lif, Tunisia

[d]QFM-UC, Department of Chemistry, University of Coimbra, Coimbra, Portugal

† Electronic supplementary information (ESI) available: Experimental details including synthesis, experimental procedure and supporting data. See DOI: 10.1039/c8ta01906a

Published on 11 May 2018. Downloaded by Universidade de Coimbra on 12/19/2018 4:16:09 PM.

difference in **1–3** (Fig. 1a) upper rims is meant to provide the sensors with different selectivity. **1** supports bulky *tert*-butyl groups on the benzene rings, **2** has free benzene rings, and **3** bears long carbon chains on the upper rim. Among the well-established gas sensing materials such as Ga_2O_3, In_2O_3, SnO_2, TiO_2, ZnO, and WO_3 and which have shown excellent performance in detecting hydrogen gas at low concentrations, TiO_2 is selected, thanks to its valuable properties of being cheap, chemically stable, and nontoxic, and the reason that its electrical resistance could vary upon adsorption of gas.[23–28] TiO_2NRs with their unique size-dependent photo-physical and electrochemical properties are expected to exhibit excellent signal amplification and transduction as compared to TiO_2NPs. The size and geometrical building of NRs and NTs increase the overall photo-conversion efficiency[29–31] and lead to a photoanodic response almost 10 times higher than that of the TiO_2NPs.[32]

Herein, we report for the first time the advantageous use of ordered CAs for creating low-cost, stable, non-toxic titania functional materials influenced by thermal variations and mutual interactions and with desirable high sensing performance for H_2 gas and for the pesticide profenofos (PFF) at RT. The as-prepared advanced materials hold stimuli-responsive adjustable surfaces, which may give rise to a new generation of sensors with controlled sensing properties.

Self-organized, vertically oriented TiO_2NR layers were grown on FTO using a hydrothermal method.[33] TiO_2NTs were prepared on a Ti substrate by an anodic oxidation procedure.[34] Both materials were employed as 3D conducting surfaces. The XRD patterns of the as-prepared 3D nanomaterials (Fig. 2a) evidence highly crystalline TiO_2NRs grown along the (001) direction perpendicular to the FTO,[33,35] and which adopt the same rutile phase of the SnO_2 surface characterized by (110), (101), (211), (002), (310), and (112) peaks at 26.50, 36.08, 54.58, 61.72, 62.82, and 69.00°, respectively.[36] Anatase TiO_2NTs are characterized by (101), (020), (105), and (121) peaks at 25.30, 47.94, 54.0, and 54.83°, respectively.[37] The comparison of the rutile and anatase irreducible representations allows us to differentiate them by the number of bands and their symmetries. Actually, the Raman spectra of TiO_2NRs and TiO_2NTs (ESI, Fig. S1†) show typical Raman bands of the rutile phase at 146, 235, 446, 612, and 825 cm^{-1},[33,38] and major bands of the anatase phase at 146, 197, 396, 516, 519, and 636 cm^{-1}, respectively.[39] Similarly in the IR range, the bands (ESI, Fig. S1† inset) observed at 384, 423, 486, and 630 cm^{-1} are assigned to the three IR modes of rutile TiO_2NRs, while those of anatase TiO_2NTs appear at 654, 534,

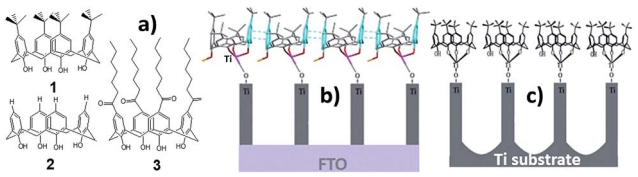

Fig. 1 Molecular structures of CAs **1–3** (a). Depiction of **1**@TiO_2NRs (b) and **1**@TiO_2NTs (c) [rod/tube tip functionalization is depicted for clarity].

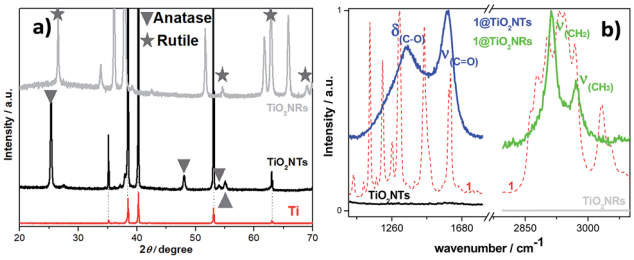

Fig. 2 XRD patterns of Ti, TiO_2NTs, and TiO_2NRs (a). Normalized Raman spectra of TiO_2NTs, TiO_2NRs, **1**, **1**@TiO_2NRs, and **1**@TiO_2NTs (b).

and 841 cm^{-1}.[40–42] Besides phase characterization, IR spectroscopy (ESI, Fig. S2†) allows surface analysis and reveals water adsorption on the TiO_2 surface through hydrogen bonding between surface OH groups and water molecules (ν(OH) centered at 3380 and 3336 cm^{-1} and $\delta(H_2O)$ at 1632 and 1639 cm^{-1}, respectively in TiO_2NRs and TiO_2NTs).[43,44] The FTO-coated glass substrate is uniformly covered with vertically and slantingly aligned 0.7 μm length rectangular hexahedrons (TiO_2NRs) (Fig. 3a) with square top facets (150 to 170 nm). TiO_2NTs are highly vertically ordered 10 nm thick cylinders of nearly 100 nm inner diameter (Fig. 3c).

CAs **1–3** were covalently grafted on the TiO_2 surface (Fig. 1b and c) by forming coordination bonds between the hydroxyl groups of CAs and surface Ti atoms, which restricts CAs to a "cone" conformation.[45] SEM analysis (Fig. 3b and d) shows CA nano-aggregates causing overlap of nanorod arrays and filling the porosities of nanotube arrays. Similar but less significant changes occur upon grafting **2** and **3** on TiO_2NRs (ESI, Fig. S3†). The high magnification micrograph (Fig. 3d) shows the accumulation of **1** on both surface sides of TiO_2NTs, thus increasing the nanotube thickness up to 34 nm. The CA layer enhances surface hydrophobicity as indicated by the change in the contact angle (ESI, Fig. S4†). The successful grafting of CAs is first characterized using Raman spectra showing $\nu(CH_3)$ and $\nu(CH_2)$ stretching vibrations in **1,3**@TiO_2NRs (Fig. 2b, ESI, Fig. S5†). By correlation with the vibrational modes of **1**, $\nu(CH_3)$ values are reduced (by 2.7-fold and 1.8-fold, respectively) and red-shifted by 4 cm^{-1} while $\nu(CH_2)$ values are ~30 cm^{-1} red-shifted and reduced (by 1.5-fold and 1.3-fold, respectively) compared to the corresponding wavenumbers in **1** and **3**, respectively, thus suggesting a different environment near the CA platform.[46] Similarly, the Raman spectrum of **1**@TiO_2NTs (Fig. 2b) identifies C–O bending and C=C stretching vibrations in **1**.[46] ν(C=C) is 16 cm^{-1} red-shifted when compared to its wavenumber in **1** (1611 cm^{-1}) evoking a conjugation between

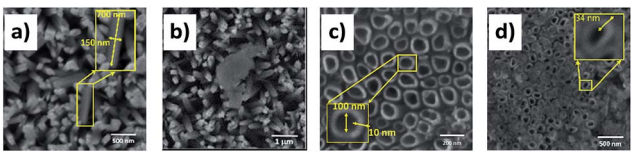

Fig. 3 Top surface SEM images of TiO_2NRs (a), **1**@TiO_2NRs (b), TiO_2-NTs (c), and **1**@TiO_2NTs (d).

 This journal is © The Royal Society of Chemistry 2018

Published on 11 May 2018. Downloaded by Universidade de Coimbra on 12/19/2018 4:16:09 PM.

neighboring two CA units *via* π–π stacking, and the creation of ground-state dimers that absorb visible blue light (460 nm – ESI, Fig. S6†) akin to those reported earlier.[46–48] The as-created dimers will trigger TiO_2 sensitization in the visible light.[45] Incorporation of CAs into the coordination sphere of surface Ti-atoms deforms the surface TiO_6 octahedron causing a shift of the phonon spectra of the TiO_2 surface by 8 cm^{-1} towards high frequencies (ESI, Fig. S7†)[49] and producing a uniform lattice strain evidenced by 0.1° shift of diffraction lines to lower angles (ESI, Fig. S8†).[50] The one difficulty that may be encountered in identifying surface deposits from their diffraction patterns is caused by the fact that the individual crystals of such deposits are often preferentially oriented with respect to the surface on which they lie. The result is a marked difference between the observed relative intensities of the diffraction lines of **1–3**@TiO_2NRs and those given for the corresponding TiO_2NRs (ESI, Fig. S9†).[50] The solid state array of CAs adsorbed on the surface can then easily be tuned by external stimuli such as pressure, heat, and vapor.[46,48] These unique features would provide potential applications for smart materials.[51] Such achievement if conceived for CA@TiO_2NRs or CA@TiO_2NTs would open new horizons towards smart sensors with a tuned surface and modulated sensing properties. **1**@TiO_2NTs were slowly cooled from 310 to 50 K and were monitored by fluorescence spectroscopy (Fig. 4a). The 340 nm band, assigned to the aryl moiety (monomer) emission,[46–48] is evidence of the interaction between **1** and TiO_2. Both bands at 340 and 461 nm can be ascribed to the disordered and ordered structures of CAs, respectively, akin to the observed temperature dependence of the fluorescence of a poly(di-*n*-hexylsilane)/TiO_2 nanoparticle hybrid film.[52] The red-shift of the central band at 461 nm by 25 nm (band at 486) hints at the rearrangement of **1** in a different crystalline order[48] leading to new diffraction peaks at 21.40, 23.08, 23.80, 27.48, 31.44, 36.02, 43.24, 47.58, 48.54, and 57.44° (Fig. 4b). The emergence of the 514 nm band suggests CAs to adopt distinct organizations at 50 K. The broadening and intensification of the emission of the tuned surface is anticipated to enhance TiO_2 sensitization and, consequently, is regarded as the original simple procedure for modulating/improving the detection response of **1**@TiO_2NTs. One can notice that this appealing procedure cannot be applied for previously reported calixarenes randomly anchored on TiO_2 particles.[53,54]

To investigate the performance of CA@TiO_2NR films for H_2 sensing, TiO_2NRs and **1–3**@TiO_2NRs were exposed to vacuum at RT until a steady baseline resistance was achieved. Next, H_2 was injected into the chamber at a constant flow rate and the resistance of the sensor was recorded every 2 s, until the steady resistance was achieved. The resistances of **1–3**@TiO_2NRs (200, 675, and 319 Ω, respectively) were higher than that of 58 Ω obtained for pure TiO_2NRs samples in a vacuum (Fig. 5a). They decreased significantly with increase in the concentration of H_2, while the TiO_2NR sensor shows a relatively slow decrease. The enhanced response/sensitivity of the **1–3**@TiO_2NR sensors (Fig. 5a inset) 21–33% may be attributed to the porous structure of CAs (Fig. 5b), which allows diffusion of H_2 inside the film.[22] Different mechanisms have been proposed for the diffusion of guest H_2 such as based on the slippage of CA layers[55] or rotation of *tert*-butyl groups like turnstiles to direct guests through the solid.[56] **1** and **2** accelerate H_2 diffusion, yielding a fast response (resistance reaches a plateau at low pressure: 3.2 and 5.6 bar, respectively) as compared to **3** (plateau reached at a high pressure of 21 bar). Conversely, the response of TiO_2NRs in the absence of CAs is ineffective (resistance reaches a plateau at a high pressure of 16 bar with low 8% sensitivity). The dissimilar behavior of **1–3** may be caused by the structural and dynamic properties highlighted earlier with H_2-CA occupancy.[57,58] **1** with the largest pore size (3.83 Å) allows maximum diffusion of H_2, and hence, forces **1**@TiO_2NRs to reach the saturation first. **2** with a smaller (3.45 Å) but most accessible

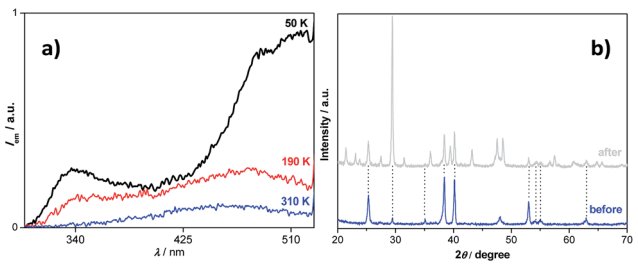

Fig. 4 Fluorescence spectra of **1**@TiO_2NTs at different temperatures (a). XRD patterns of **1**@TiO_2NTs before and after thermal treatment (b).

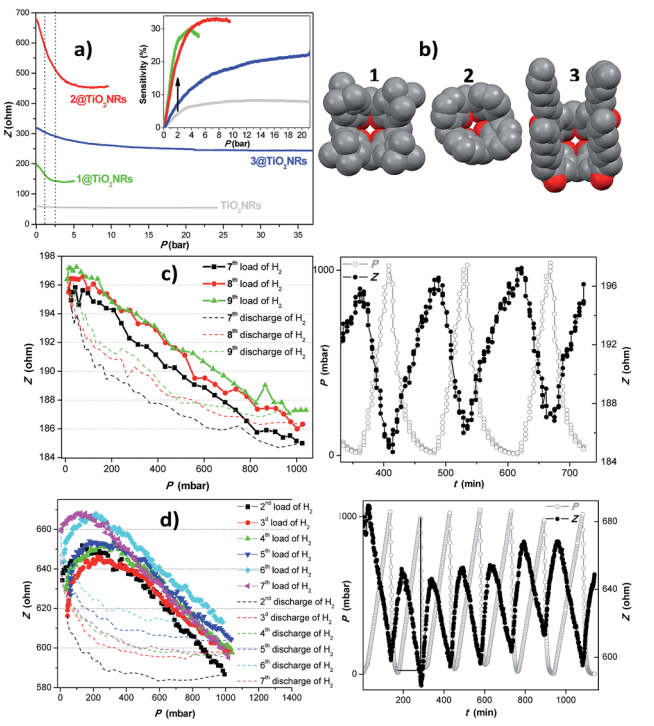

Fig. 5 Variation of the resistance of **1–3**@TiO_2NRs [inset: sensitivity of H_2 sensors] with hydrogen pressure at 290 K (a) [S is the sensitivity, R_0 is the stable sensor resistance in a vacuum, R_H is the stable sensor resistance after the hydrogen injected. $S = \frac{|R_H - R_0|}{R_0}$]. Pores **1**, **2**, and **3** (b). Resistance variation in **1**@TiO_2NRs with a series of loads at 1 bar and discharge of hydrogen at 290 K (c). Resistance variation in **2**@TiO_2NRs with a series of loads at 1 bar and discharge of hydrogen at 290 K (d).

Published on 11 May 2018. Downloaded by Universidade de Coimbra on 12/19/2018 4:16:09 PM.

pore size is slightly less efficient. However, although **3** has a large pore size (3.78 Å) it decreases H_2 diffusion most probably because its bulky chains reduce access to pores.

The results indicate that the mechanism behind this unusual enhancement of conductance (decrease of resistance) in CA@TiO_2NRs with pure hydrogen exposure is neither the reduction of the titania lattice[59,60] nor the removal of chemisorbed oxygen (not present in the high-pressure chamber) from the nanorod surface by the hydrogen[61] nor the well-known spillover mechanism of hydrogen by platinum[62,63] (silver electrodes are used instead. The direct adsorption of hydrogen on the silver surface has no significant role in the hydrogen detection[64]), but the supported calixarenes are essential as they may act as Ru_{10} clusters and favor the spontaneous dissociation of H_2,[65] a process which does not occur on the bare oxide surface.[66] Upon adsorption of several H_2 molecules on the Ru_{10} metal cluster, it becomes thermodynamically favorable for hydrogen transfer from the metal to the O sites of the oxide surface. The migration of an H atom from the Ru cluster to the surface is accompanied by an electron transfer to the empty states of the support with reduction of the oxide surface. Calixarene-causing chemisorption of the spilled-over hydrogen atoms on the nanorod surface, which make a partial charge transfer to the titania, thereby creating an electron accumulation layer on the nanorod surface can be considered as a more probable reason to enhance the electrical conductance. Finally, **1**@TiO_2NR and **2**@TiO_2NR sensors deliver a linear and reproducible response (response/recovery times remain constant after several loads of H_2) when H_2 is injected at 1 bar at 290 K (Fig. 5c and d) and are regenerated by spontaneous H_2 removal, which evidence a long-time stability of the sensors. Therefore, they will be ideal components for low-cost handy devices for the detection of H_2. The prominence of these sensors is again strengthened by their opposite response (resistance increases) with an increase in the concentration of N_2 (ESI, Fig. S10†), which leads to accurate selective detection.

In another contextual application we investigated the performance of CA@TiO_2NR films as sensors for profenofos. The current density variation as a function of the voltage was measured for TiO_2NRs, **1**@TiO_2NRs, and for PFF@**1**@TiO_2NRs under artificial solar light illumination (Fig. 6a) in the range between the reduction and the oxidation potentials of TiO_2. In the absence of applied potential, the current density of TiO_2NRs is enhanced 4-fold in **1**@TiO_2NRs due to CA-driven visible-light sensitization of TiO_2 and through ligand to metal charge transfer between **1** and Ti centers on the surface.[45] The current density is verified to result from photon excitation as no current was registered in the dark (Fig. 6a inset). **1**@TiO_2NRs were immersed for 1 min in a PFF solution at RT and then the current density was measured. Interestingly, the intensity of the current density is amplified 6-fold due to the inclusion of PFF in the cavity of **1**.[12] Effective detection of PFF is complemented by efficient solid capture which prevents its discharge into the electrolyte solution during current density measurements. The synergy of the two properties is at the origin of our current challenge to fabricate handy sensors. The strong immobilization of PFF on **1**@TiO_2NRs is caused by intermolecular

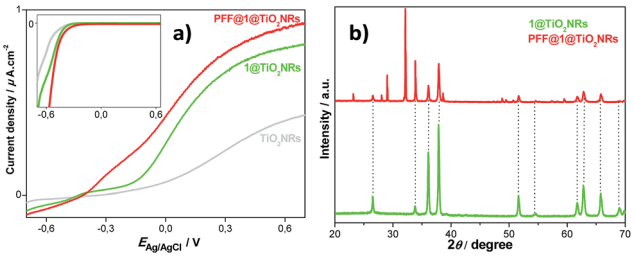

Fig. 6 Photocurrent density *vs.* voltage curves of TiO_2NRs, **1**@TiO_2NRs, and PFF@**1**@TiO_2NRs under xenon lamp illumination (a) and in the dark [inset]. XRD patterns of **1**@TiO_2NRs and PFF@**1**@TiO_2NRs (b).

interactions with **1**, is characterized by its vibrational bands at 994, 1102, 1133, and 1154 cm^{-1} in the Raman spectrum (ESI, Fig. S11†), and forms a SAM that is observed under an optical microscope (ESI, Fig. S12†) and is characterized by an XRD pattern (Fig. 6b) showing new diffraction peaks at 23.15, 28.0, 29.0, 32.13, and 38.62°. The possibility of performing surface chemistry tailoring with SAMs constitutes a versatile approach towards the tuning of the electronic and morphological properties of the interfaces relevant to the response of our sensor, and gives rise to completely new types of behaviors that open unprecedented applications.[67]

Conclusions

In conclusion, we have developed an effective strategy to improve sensing performance at RT for the fabrication of ideal components for low-cost handy devices for rapid and sensitive detection of gases H_2 and N_2 and analyte PFF. The components are CA functionalized TiO_2NR/TiO_2NT semiconductors. Neighboring CAs form, *via* π–π stacking, dimers that absorb blue light and trigger TiO_2 sensitization in the visible light. Thanks to their unique supramolecular chemistry, grafted CAs create SAMs that switch order under a thermal stimulus, thus transforming the semiconductor into a stimuli-responsive material and promoting modulated sensing properties. The advantageous porous structure of CAs allows diffusion of H_2 inside TiO_2NRs which, subsequently, yields a fast, linear, sensitive, and reproducible response at RT. The as-designed sensors show opposite response for H_2 (resistance decreases) and N_2 (resistance increases). Moreover, the excellent inclusion behavior of CAs triggers strong capture and then detection of PFF and promotes their self-organization onto surfaces.

Conflicts of interest

There are no conflicts to declare.

Acknowledgements

This work was supported by funds from FEDER, from FCT-the Portuguese Foundation for Science and Technology under the Projects No. UID/MULTI/00070/2013 and UID/FIS/04564/2016, and from MESRS-the Tunisian Ministry of Higher Education

 This journal is © The Royal Society of Chemistry 2018

Published on 11 May 2018. Downloaded by Universidade de Coimbra on 12/19/2018 4:16:09 PM.

and Scientific Research. Access to the TAIL-UC facility funded under QREN-Mais Centro Project No. ICT_2009_02_012_1890 is gratefully acknowledged. Prof. Luísa Durães and Prof. Sérgio Seixas de Melo are acknowledged for providing assistance in contact angle and in absorbance measurements. IO is thankful to Prof. Radhouane Chtourou for encouragement and to Prof. Hugh Burrows and Prof. Mounir Dhouib for a critical reading of the manuscript.

Notes and references

1 K. Ariga, J. Li, J. Fei, Q. Ji and J. P. Hill, *Adv. Mater.*, 2016, **28**, 1251–1286.
2 X. Ma, H. Tang, P. S. Malcampo and E. Galoppini, *Curr. Org. Chem.*, 2017, **21**, 2324–2337.
3 M. Liua, X. Dinga, Q. Yanga, Y. Wanga, G. Zhaoa and N. Nianjun Yangb, *J. Hazard. Mater.*, 2017, **331**, 309–320.
4 H. Shi, Y. Wang, J. Zhao, X. Huang and G. Zhao, *J. Hazard. Mater.*, 2018, **342**, 131–138.
5 F. Wang, Y. Yang and T. M. Swager, *Angew. Chem., Int. Ed.*, 2008, **47**, 8394–8396.
6 L. Mutihac, J. H. Lee, J. S. Kim and J. Vicens, *Chem. Soc. Rev.*, 2011, **40**, 2777–2796.
7 Y. Sun, J. Ma, D. Tian and H. Li, *Chem. Commun.*, 2016, **52**, 4602–4612.
8 X. Zhou, S. Han, Q. Zhang, Y. Dou, J. Guo, L. Che and J. Zhang, *Polym. Chem.*, 2015, **6**, 3716–3727.
9 J. Zhou, M. Chen, J. Xie and G. Diao, *ACS Appl. Mater. Interfaces*, 2013, **5**, 11218–11224.
10 X. Mao, D. Tian and H. Li, *Chem. Commun.*, 2012, **48**, 4851–4853.
11 F. Zhang, Y. Sun, D. Tian, W. S. Shin, J. S. Kim and H. Li, *Chem. Commun.*, 2016, **52**, 12685–12693.
12 H. Shi, G. Zhao, T. Cao, M. Liu, C. Guan, X. Huang, Z. Zhu, N. Yang and O. A. Williams, *Electrochem. Commun.*, 2012, **19**, 111–114.
13 Y. Luo, C. Zhang, B. Zheng, X. Geng and M. Debliquy, *Int. J. Hydrogen Energy*, 2017, **42**, 20386–20397.
14 A. Monamary and K. Vijayalakshmi, *J. Mater. Sci.: Mater. Electron.*, 2018, **29**, 5316–5326.
15 Z. Wang, Z. Li, T. Jiang, X. Xu and C. Wang, *ACS Appl. Mater. Interfaces*, 2013, **5**, 2013–2021.
16 C. Xiang, Z. She, Y. Zou, J. Cheng, H. Chu, S. Qiu, H. Zhang, L. Sun and F. Xu, *Ceram. Int.*, 2014, **40**, 16343–16348.
17 R. Yatskiv, J. Grym, P. Gladkov, O. Cernohorsky, J. Vanis and J. Maixner, *Solid-State Electron.*, 2016, **116**, 124–129.
18 D. Zhang, Y. Sun, C. Jiang and Y. Zhang, *Sens. Actuators, B*, 2017, **242**, 15–24.
19 C. Ling, Q. Xue, Z. Han, Z. Zhang, Y. Du and Y. Liu, *Sens. Actuators, B*, 2014, **205**, 255–260.
20 W. Chen, Y. Xiong, Y. Li, P. Cui, S. Guo and W. Chen, *Int. J. Hydrogen Energy*, 2016, **41**, 3307–3312.
21 J. Zhang, X. Liu, G. Neri and N. Pinna, *Adv. Mater.*, 2016, **28**, 795–831.
22 S. Kumar, S. Chawla and M. C. Zou, *J. Inclusion Phenom. Macrocyclic Chem.*, 2017, **88**, 129–158.
23 N. N. Greenwood and A. Earnshaw, *Chemistry of the Elements*, Elsevier Science, 2nd edn, 1997.
24 D. Sett and D. Basak, *Sens. Actuators, B*, 2017, **243**, 475–483.
25 Z. Q. Zheng, L. F. Zhu and B. Wang, *Nanoscale Res. Lett.*, 2015, **10**, 239.
26 S. S. Kalanur, I. H. Yoo, Y. A. Lee and H. Seo, *Sens. Actuators, B*, 2015, **221**, 411–417.
27 T. Li, W. Zeng, D. F. Shi and S. Hussain, *Mater. Lett.*, 2015, **161**, 648–651.
28 S. Nakagomi, T. Sai and Y. Kokubun, *Sens. Actuators, B*, 2013, **187**, 413–419.
29 C. N. Ram Rao and A. Govindaraj, *Nanotubes and Nanowires*, Royal Society of Chemistry, 2011.
30 M. Paulose, K. Shankar, S. Yoriya, H. E. Prakasam, O. K. Varghese, G. K. Mor, T. A. Latempa, A. Fitzgerald and C. A. Grimes, *J. Phys. Chem. B*, 2006, **110**, 16179–16184.
31 N. N. Bwana, *Nano Res.*, 2008, **1**, 483–489.
32 J. H. Park, S. Kim and A. J. Bard, *Nano Lett.*, 2006, **6**, 24–28.
33 W. Chakhari, J. Ben Naceur, S. Ben Taieb, I. Ben Assaker and R. Chtourou, *J. Alloys Compd.*, 2016, **708**, 862–870.
34 S. Ben Taieb, T. N. Pham Truong, S. Chaguetmi, J. Ben Naceur, A. Bardaoui, M. Gannouni, P. Decorse, L. Mouton, S. Nowak, F. Mammeric, R. Chtourou and S. Ammar, *J. Photochem. Photobiol., B*, 2016, **40**, 337–344.
35 B. Liu and E. S. Aydil, *J. Am. Chem. Soc.*, 2009, **131**, 3985–3990.
36 D. A. H. Hanaor and C. C. Sorrell, *J. Mater. Sci.*, 2011, **46**, 855–874.
37 M. N. Khan and J. Bashir, *J. Mod. Phys.*, 2011, **2**, 962–965.
38 A. Chaves, R. S. Katiyar and S. P. S. Porto, *Phys. Rev.*, 1974, **10**, 3522–3533.
39 T. Ohsaka, F. Izumi and Y. Fujiki, *J. Raman Spectrosc.*, 1978, **7**, 321–324.
40 W. B. White, *Mater. Res. Bull.*, 1967, **2**, 381–394.
41 G. Busca, G. Ramis, J. M. Gallardo Amores, V. S. Escribano and P. Piaggio, *J. Chem. Soc., Faraday Trans.*, 1994, **90**, 3181–3190.
42 R. J. Gonzalez, R. Zallen and H. Berger, *Phys. Rev. B*, 1996, **55**, 7014–7017.
43 B. Erdem, R. A. Hunsicker, G. W. Simmons, E. D. Sudol, V. L. Dimonie and M. S. El-Aasser, *Langmuir*, 2001, **17**, 2664–2669.
44 H. N. Chuang, J. S. Bow, Y. Zheng, S. Y. Chen, N. J. Ho and P. Shen, *Nanoscale Res. Lett.*, 2010, **5**, 972–985.
45 J. M. Notestein, E. Iglesia and A. Katz, *Chem. Mater.*, 2007, **19**, 4998–5005.
46 I. Oueslati, J. A. Paixao, A. Shkurenko, K. Suwinska, J. S. Seixas de Melo and L. A. E. Batista de Carvalho, *J. Mater. Chem. C*, 2014, **2**, 9012–9020.
47 I. Oueslati, A. W. Coleman, B. de Castro and M. N. Berberan-Santos, *J. Fluoresc.*, 2008, **18**, 1123–1129.
48 I. Oueslati, J. A. Paixao, V. H. Rodrigues, A. Shkurenko, B. Lesniewska, K. Suwinska, M. A. Eusebio, T. M. Maria and J. S. Seixas de Melo, *J. Phys. Chem. C*, 2014, **118**, 13118–13125.
49 T. Bezrodna, G. Puchkovska, V. Shymanovska, J. Baran and H. Ratajczak, *J. Mol. Struct.*, 2004, **700**, 175–181.

Published on 11 May 2018. Downloaded by Universidade de Coimbra on 12/19/2018 4:16:09 PM.

50 B. D. Cullity, *Elements of X-ray diffraction*, Addison-Wesley Publishing Company, Inc., 1956.
51 I. Oueslati, *Curr. Org. Chem.*, 2015, **19**, 2309–2320.
52 A. Watanabe, T. Miyashita, A. Kasuya, M. Takahashi and Y. Kawazoe, *Polymer*, 2008, **49**, 554–560.
53 S. Akın, M. Gülen, S. Sayın, H. Azak, H. B. Yıldız and S. Sonmezoglu, *J. Power Sources*, 2016, **307**, 796–805.
54 B. J. Waghmode, Z. Husain, M. Joshi, S. D. Sathaye, K. R. Patil and D. D. Malkhede, *J. Polym. Res.*, 2016, **23**(35), 2–11.
55 G. D. Enright, E. B. Brouwer, P. A. Halchuk, K. J. Ooms, M. J. Ferguson, K. A. Udachin and J. A. Ripmeester, *Acta Crystallogr., Sect. A: Found. Crystallogr.*, 2002, **58**, c310.
56 G. S. Ananchenko, K. A. Udachin, M. Pojarova, S. Jebors, A. W. Coleman and J. A. Ripmeester, *Chem. Commun.*, 2007, **7**, 707–709.
57 S. Alavi and J. A. Ripmeester, *Chem.–Eur. J.*, 2008, **14**, 1965–1971.
58 S. Alavi, N. A. Afagh, J. A. Ripmeester and D. L. Thompson, *Chem.–Eur. J.*, 2006, **12**, 5231–5237.
59 R. D. Shannon, *J. Appl. Phys.*, 1964, **35**, 3414–3416.
60 K. H. Kim, E. J. Ju and J. S. Choi, *J. Phys. Chem. Solids*, 1984, **45**, 1265–1269.
61 R. M. Walton, D. J. Dwyer, J. W. Schwank and J. L. Gland, *Appl. Surf. Sci.*, 1998, **125**, 199–207.
62 U. Roland, T. Braunschweig and F. Roessner, *J. Mol. Catal. A: Chem.*, 1997, **127**, 61–84.
63 O. K. Varghese, D. Gong, M. Paulose, K. G. Ong, E. C. Dickey and C. A. Grimes, *Adv. Mater.*, 2003, **15**, 624–627.
64 S. Rahbarpour and S. M. Hosseini-Golgoo, *Schottky Type Ag–TiO_2 Hydrogen Sensor: Gas Sensing Mechanism and Modeling*, Nürnberg/Nuremberg, Germany, 2012.
65 H.-Y. T. Chen, S. Tosoni and G. Pacchioni, *ACS Catal.*, 2015, **5**, 5486–5495.
66 U. Roland, R. Salzer, T. Braunschweig, F. Roessner and H. Winkler, *J. Chem. Soc., Faraday Trans.*, 1995, **91**, 1091–1095.
67 S. Casalini, C. A. Bortolotti, F. Leonardic and F. Biscarini, *Chem. Soc. Rev.*, 2017, **46**, 40–71.

 This journal is © The Royal Society of Chemistry 2018